# Insight into Continuum couplings

F.M. Nunes[a], A.M. Mukhamedzhanov[b], C.C. Rosa[c], B. Irgaziev[d] *

[a] NSCL and Department of Physics and Astronomy Michigan State University, East Lansing MI 48824 USA

[b] Cyclotron Institute, Texas A& M University, College Station, TX 77843, USA

[c]Faculdade de Ciencias, INESC-Porto, Porto, Portugal

[d]Physics Department, National University, Tashkent 700174, Uzbekistan

Motivated by the large application of the CDCC method (continuum discretized coupled channel method) to reactions with dripline nuclei of two body nature $A = c + p$, we study the behaviour of these couplings for a low energy breakup scenario, where they play a crucial role. Continuum couplings can produce a variety of effects on reaction observables. Based on previous calculations, we investigate their range and their dependence on the relative angular momentum and the relative energy between the pair. The conclusions of this work can help design a more efficient model space for the two body continuum.

## 1. Motivation

Due to the very weak binding of halo nuclei, breakup channels typically have a preponderant role in the reaction process. In the language introduced by the Continuum Discretization Coupled Channels (CDCC) method [1–3], one could say that the ground state (g.s.) of these loosely bound systems *couple strongly to the continuum*, which essentially means that the projectile breaks up easily. Clearly, the details of the coupling operator determined by the physical process that excites the initial bound state into the continuum, is a relevant factor, together with the internal Hamiltonian of the projectile.

One of the simplest processes we can consider is the electromagnetic excitation $A+\gamma \rightarrow c + p$ (photo-absorption), which in turn is related to the inverse process, the radiative capture c(p,$\gamma$)A. The multipole electric couplings were previously studied in connection to Astrophysics [4], specifically for proton capture reactions. Therein, E1 and E2 couplings connecting the ground state and the scattering state of the proton attached to an inert core were described in detail, as well as the identification of the various ingredients contributing to the general pattern. It was found that the behaviour close to zero energy is not solely determined by the nearby pole (corresponding to the c-p binding energy). It depends on

*This work has been partially supported by Fundação para a Ciência e a Tecnologia (F.C.T.) of Portugal, under the grant POCTIC/36282/99, by the NSCL at Michigan State University, by the U. S. Department of Energy under Grant No. DE-FG03-93ER40773 and the U. S. National Science Foundation under Grant No. PHY-0140343

the interplay of various effects including both bound state and scattering state centrifugal barriers, the Coulomb barrier, etc. The multipole couplings going into a capture cross section calculation can be written as:

$$V_\lambda(E) \;=\; < \phi_{E_{rel}}(r)|r^\lambda Y_\lambda(\hat{\mathbf{r}})|\phi_{gs}(r) >, \qquad (1)$$

where $\hat{\mathbf{r}} = \mathbf{r}/r$ is a unit vector, $\phi_{gs}(r)$ is the bound wavefunction of the nucleus A, $\phi_{E_{rel}}(r)$ is the scattering state of $p + c$ moving with the relative kinetic energy $E_{rel}$. Although not essential, for simplicity we shall assume that the only bound state of nucleus A is the ground state. This is typically the case for nuclei on the dripline.

When considering other reactions with exotic beams, the couplings to the continuum are often referred to as a crucial ingredient. Breakup reactions epitomize the radical effect that couplings to the continuum may have [5]. Of particular importance was the finding that continuum-continuum couplings could decrease the cross section by large factors. For instance, in the breakup reaction of $^8$B on $^{56}$Ni at near barrier energies, a large peak in the differential cross section is produced within a 1-step calculation, whereas in a full coupled channel model including continuum-continuum couplings, the peak is so weak that it is hardly visible [6–9], in agreement with experiment [10]. Even earlier, in the studies of deuteron breakup, such continuum effects were shown to play a role [11,12]. In opposition, recent breakup calculations of $^8$B on other targets and different energy regimes reveal minor continuum-continuum effects [13,14]. So, what makes continuum-continuum effects important in the reaction mechanism? What are the decisive ingredients? The theoretical predictions using CDCC (e.g. [7]) rely on large scale calculations where virtually all relevant energies and partial waves of the *core* + $p$ system are included. Hundreds of radial wavefunctions are contributing to the final result and the effect obviously becomes everything but transparent. Is there an intuitive picture that can justify such a forceful effect? This work tries to shed light on these issues.

In the first part (section II) we present some theoretical considerations and set up the input needed for the calculations. Next, in section III, we consider couplings from the ground state into the continuum. Section IV concerns continuum-continuum couplings for different combinations of initial and final angular momenta. Comments and conclusions can be found in section V.

## 2. Theoretical considerations

The reaction of a loosely bound projectile ($A = c+p$) with a target $T$ can be described within a three-body model by two dynamical variables represented in Fig.(1): $\mathbf{R}$ the distance between the target and the center of mass of the projectile, and $\mathbf{r}$ the distance between the core and the valence particle in the projectile. The conjugates of these two coordinates $(\vec{r}, \vec{R})$ are the corresponding momenta $(\vec{k}, \vec{K})$. The potential couplings we are interested in will ultimately consist of an overlap between an initial and a final scattering wave with energies $E^i_{rel} = \hbar^2 k_i^2/(2\mu_{cp})$, and $E^f_{rel} = \hbar^2 k_f^2/(2\mu_{cp})$, respectively ($\mu_{cp}$ being the reduced mass of the core-p system). Since the wavelength of the scattering states depend on the corresponding energies $E^i_{rel}$ and $E^f_{rel}$, one might expect to find a maximum overlap when these energies are similar.

Let us then consider the breakup of $A = c+p$ on a target $T$. The exact solution to this three-body problem can be achieved by solving the Faddeev equations [15]. Alternatively,

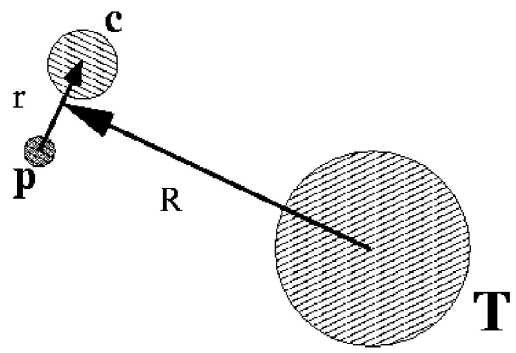


Figure 1. Coordinates used in the reaction description.

one can expand the three body wavefunction in terms of the relative motion of $c+p$ $[\phi_k(r)]$ and that of the projectile and the target $A+T$ $[f_K(R)]$. If one further discretizes the continuum by taking a set of representative energies for $c+p$, $E^i_{rel}$ $(i=1,...,N)$, the three body wavefunction can be written as

$$\Psi_K(r,R) = \sum_{\alpha=0}^{N} \frac{\phi_\alpha(r)}{r} f_{\alpha K}(R). \tag{2}$$

Here the subscript $\alpha$ runs over the set of energy values $E^\alpha_{rel}$ and angular momentum combinations ($\alpha=0$ corresponds to the projectile in the g.s.).

Introducing this expansion in the Schrödinger equation, and working out the angular parts, one can arrive at the following coupled radial differential equations:

$$\left[-\frac{\hbar^2}{2\mu}\left(\frac{d^2}{dR^2} - \frac{\mathcal{L}(\mathcal{L}+1)}{R^2}\right) + E^\alpha_{rel} - E_s\right] f_\alpha(R) + \sum_{\alpha'} i^{\mathcal{L}'-\mathcal{L}}\, V_{\alpha\alpha'}(R) f_{\alpha'}(R) = 0, \tag{3}$$

where $E_s$ is the relative energy of the projectile $A$ and target $T$ ($E_s = \frac{\hbar^2 K^2}{2\mu_{AT}}$) and $E^\alpha_{rel}$ is the relative energy of $c+p$ for the particular discretization chosen ($E^0_{rel} = -\varepsilon < 0$ for its ground state). The full solution of the coupled equations (Eq. 3) provides the CDCC scattering amplitudes needed to calculate the reaction process. Instead of solving the full coupled channel equations, one can approach a solution iteratively. In the 1-step calculation, the only couplings included are the couplings connecting the g.s. of nucleus $A$ and the final scattering state $c+p$, given by:

$$V_{\alpha;0}(\mathbf{R}) \;=\; < \frac{\phi_\alpha(\mathbf{r})}{r} | V_{cT}(R_c) + V_{pT}(R_p) | \frac{\phi_0(\mathbf{r})}{r} > \;. \tag{4}$$

$V_{cT}(R_c)$ and $V_{pT}(R_p)$ are the total (nuclear and Coulomb) interactions between $c-T$ and $p-T$ systems respectively. We assume that $V_{cT}(R_c)$ and $V_{pT}(R_p)$ are central potentials. Note that $\mathbf{R}_c = \mathbf{R} + m_p/m_A\,\mathbf{r}$ and $\mathbf{R}_p = \mathbf{R} - m_c/m_A\,\mathbf{r}$. One-step calculations are often not sufficient to describe the reaction accurately and one needs to include multi-step paths,

and in particular multi-step processes within the continuum. Such a calculation involves the continuum-continuum couplings:

$$V_{\alpha;\alpha'}(\mathbf{R}) \;=\; < \frac{\phi_\alpha(\mathbf{r})}{r}|V_{cT}(R_c)+V_{pT}(R_p)|\frac{\phi_{\alpha'}(\mathbf{r})}{r} >, \tag{5}$$

where both $\phi_\alpha(\mathbf{r})$ and $\phi_{\alpha'}(\mathbf{r})$ are unbound states. In general, when these couplings are strong, iterative processes do not work and the CDCC equations (Eq.3) needs to be solved exactly.

Note that $V_{cT}(R_c)+V_{pT}(R_p)$ in Eqs. 4 and 5 depend on both coordinates, $\mathbf{R}$ and $\mathbf{r}$. The couplings represented in Eqs. 4 and 5 are integrated over $\mathbf{r}$ such that the coupling potentials $V^L_{\alpha 0}(R)$ and $V^L_{\alpha\alpha'}(R)$ depend on the relative coordinate between the c.m. of the projectile and the target $\mathbf{R}$. The angular part of these coupling potentials can be determined algebraically and is not particularly interesting for the questions we want to address. In this work we focus on the radial integral only, as it contains the behavioural information we are searching for. The standard multipole expansion of the potential $V_{cT}(R_c)+V_{pT}(R_p)$ in spherical harmonics is:

$$V_{cT}(R_c)+V_{pT}(R_p)=\sum_{LM}[V^L_{cT}(R,r)+V^L_{pT}(R,r)]Y_{LM}(\hat{\mathbf{R}})Y^*_{LM}(\hat{\mathbf{r}}), \tag{6}$$

where $V^L_{cT}(R,r)$ and $V^L_{pT}(R,r)$ are invariant radial potential multipole components. From here, we get the invariant radial potentials for the bound state-continuum couplings

$$V^L_{\alpha;0}(R) \;=\; < \frac{\phi_\alpha(r)}{r}|V^L_{cT}(R,r)+V^L_{pT}(R,r)|\frac{\phi_0(r)}{r} > , \tag{7}$$

and for the continuum-continuum couplings

$$V^L_{\alpha;\alpha'}(R) \;=\; < \frac{\phi_\alpha(r)}{r}|V^L_{cT}(R,r)+V^L_{pT}(R,r)|\frac{\phi_{\alpha'}(r)}{r} > . \tag{8}$$

These potentials enter the coupled radial equations (Eq.3). For pure scattering waves, the radial integrals over $r$ of the continuum-continuum couplings (Eq.8) diverge as $r\to\infty$. One solution to this problem is to replace the scattering wave functions with definite energy, by wave packets averaged over energy, using energy bins [7]. Then the states become square integrable. This is a standard method used in the CDCC formalism, typically referred to as the averaging method [1–3]. In [16] a comparison between this averaging method and the mid-point method is performed for some scattering observables.

In the avergaging method, the radial bin functions $\varphi_\alpha$ are defined as a superposition

$$\varphi_\alpha(r)=\sqrt{\frac{2}{\pi N_\alpha}}\int_{k_{i-1}}^{k_i} g_\alpha(k)\phi_\alpha(k,r)\,dk \tag{9}$$

of the pure scattering states $\phi_\alpha(k,r)$, eigenstates of the $c+p$ internal Hamiltonian, with weight function $g_\alpha(k)$. Here $N_\alpha=\int_{k_{i-1}}^{k_i}|g_\alpha(k)|^2\,dk$ is a normalization constant. The $\phi_\alpha(k,r)$ are defined such that, for $r\to\infty$,

$$\phi_\alpha(k,r)\to[\cos\delta_\alpha(k)F_\ell(kr)+\sin\delta_\alpha(k)G_\ell(kr)]\ , \tag{10}$$

where $k\in\alpha$ and $F_\ell$ and $G_\ell$ are the regular and irregular partial wave Coulomb functions. So $\phi_\alpha$ is real when using a real $c+p$ two-body interaction. An optimal discretization

of the continuum requires a consideration of the number N of bins, the boundaries $k_i$, the widths $\Delta k_i$ and the weights $g_\alpha$ in the bins, which may depend on the projectile $\ell j$ configuration. Our bins are usually regular in momentum space.

Note that the product of the scattering wave functions in the integrand of Eq.(8) goes as $1/r^2$ at large distances $r \to \infty$, while, after introducing the scattering bin functions, the asymptotics fall much more rapidly $\sim 1/r^4$, providing the convergence of the continuum-continuum coupling potential $V^L_{\alpha;\alpha'}(R)$. It is worth mentioning that, although the inclusion of a tensor force in deuteron bins was performed for deuteron elastic scattering in the early nineties [17], so far, our work has been limited to bin wavefunctions generated for potentials without tensor interactions. Also the nuclear couplings involve the absorptive part of the optical potential. For simplicity, in the graphical representation, we will concentrate only on the real part of Eq.(8). We have checked that the general trend to be discussed below is maintained for the imaginary component too.

After $r$ is integrated, the long range $R$ radial dependence of these couplings will be determined by the Coulomb interaction given that the nuclear is short range. The multipole Coulomb parts of the potentials for a transition $L$ can be written as:

$$V^{CL}_{fT}(R,r) \sim \frac{r^L}{R^{L+1}},\ r < R,$$
$$V^{CL}_{fT}(R,r) \sim \frac{R^L}{r^{L+1}},\ r \geq R, \tag{11}$$

where the superscript $C$ stands for $C = Coulomb$ and the subscript $f$ stands for either of the fragments $f = core, p$.

For g.s.-continuum case, the coupling integral has an upper limit determined by the exponential fall of the bound state wavefunction:

$$V^{CL}_{\alpha;0}(R) \sim \frac{1}{R^{L+1}} \int_0^\infty dr\ r^{L+2}\ \frac{\varphi_\alpha(r)}{r} \frac{\phi_{gs}(r)}{r}\ . \tag{12}$$

It is then trivial to conclude that the long-range behaviour of the g.s.-continuum couplings is $\sim \frac{1}{R^{L+1}}$ (this is independent on whether bins are used for the scattering states or not).

As for continuum-continuum couplings, the matrix element contains essentially two integral terms:

$$V^{CL}_{\alpha;\alpha'}(R) \sim \frac{1}{R^{L+1}} \int_0^R dr\ r^{L+2}\ \frac{\varphi_\alpha(r)}{r}\ \frac{\varphi_{\alpha'}(r)}{r} + R^L \int_R^\infty dr\ r^{-L+1}\ \frac{\varphi_\alpha(r)}{r} \frac{\varphi_{\alpha'}(r)}{r} \tag{13}$$

The contribution from the lower limit of the first term gives trivially an asymptotic long range behaviour dependent on the multipolarity $1/R^{L+1}$. Since the bin wavefunction $\varphi_\alpha(r)$ falls of as $Sin(..)/r$, it is easy to see that the upper limit of the first term goes as $\sim 1/R^3$. As to the second term, there are two possibilities. The first when the momentum of the initial and final state are approximately the same (corresponding to $\alpha = \alpha'$): then the integrand of the second term reduces essentially to $\sim 1/R^{L+3}$ and the second integral goes trivially as $\sim 1/R^2$. If on the other hand the momenta differ significantly, then $|k_i - k_f|r$ is large and an expansion of the integrand in $1/qr$ (where $q = k_f - k_i$ is the transferred momentum) is appropriate. Under these conditions, one can show that the contribution of the second term goes as $\sim 1/R^3$. Note that, we considered, in these derivations, the

asymptotics $\varphi_\alpha(r)$ without Coulomb for simplicity: the Coulomb will only add oscillations and will not change the conclusions with respect to the asymptotic R-dependence. One can then write:

$$V^{CL}_{\alpha;\alpha'}(R) \sim c_1 \frac{1}{R^{L+1}} + c_2 \frac{1}{R^2} + \mathcal{O}(\frac{1}{R^3})\ \alpha = \alpha'$$
$$V^{CL}_{\alpha;\alpha'}(R) \sim c_1 \frac{1}{R^{L+1}} + c_2 \frac{1}{R^3} + \mathcal{O}(\frac{1}{R^4})\ \alpha \neq \alpha' \tag{14}$$

For couplings between different bins, the asymptotic behaviour of the dipole part is $\sim 1/R^2$ but all higher order multipoles will fall off as $\sim 1/R^3$. Below we show results for multipolarity up to $L \leq 2$. For couplings between identical bins, the behaviour for $R \to \infty$ is $\sim 1/R^2$ for all multipolarities.

Intuitively one may think that, in order to determine the importance of the couplings, it would be sufficient to compare their strength $V_{if}$ to the scattering energy. However, even after convergence of a scattering observable is obtained, couplings can be reduced significantly by reducing of the bin width further. The relationship would no longer be trivial and one possibility would be to weigh it by the total number of bins.

In the weak coupling limit one can think about Eq.(3) perturbatively, where the perturbation consists on the sum of all the couplings. From first order perturbation theory, one expects that the main effect will come from coupling states close in energy since the correction to the wavefunctions would depend on $V_{\alpha,\alpha'}/|E^i_{rel} - E^f_{rel}|$. This agrees with the expectation delineated in the beginning of this section. Nevertheless, it should be noted that in many applications, couplings are too strong to justify a pertubative approach.

The results to be discussed in the next sections are a reproduction of the couplings used in the analysis of the breakup of $^8$B on $^{58}$Ni around the Coulomb barrier [8]. The optical potential of Moroz [18] is used for the $^7$Be-$^{58}$Ni system. The proton-$^{58}$Ni potential is taken from the global parameterization of Becchetti and Greenlees (BG) [19]. The proton-$^7$Be binding potential is taken from Esbensen and Bertsch [20] after setting the spin orbit to zero. The potential used to construct the bin states is the same (real) potential as that used to bind the $^8$B ground state by 0.137 MeV, assumed a pure $p_{3/2}$ proton single-particle state. This potential produces a sharp p-wave resonance at $\approx 0.8$ MeV and a broad d-wave resonance at $\approx 3$ MeV. The energy location of the resonances are not crucial for the present study. We consider bins up to 8 MeV energy, binned up in regular momentum intervals of 0.25 fm$^{-1}$ width. The maximum radius $r$ considered for the bins is 60 fm. These are the typical parameters used in the previous CDCC model space. These parameters were checked for convergence.

Another parameter that is relevant in the CDCC calculation is the maximum relative angular momentum for the $c+p$ required. So far, calculations for the $^8$B system have required up to $l = 3$ partial waves. We will here show results up to $l = 2$. Our notation for the $c+p$ orbital momenta of the initial and final states are $l_i$ and $l_f$, respectively. Of course, for the $^8$B ground state $l_i = 1$. From now on we will discuss plots as a function of initial and final $c+p$ relative energies, which we designate by $E_i$ and $E_f$. The above mentioned calculations [8] were performed for an incident projectile energy of $E_s = 26$ MeV. This value does no enter in the present study.

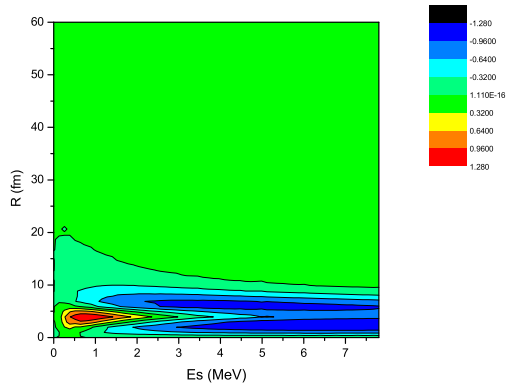


Figure 2. Contour plot of the dipole coupling matrix elements between an $l_f = 0$ scattering state and the g.s., as a function of the relative energy p-$^7$Be and R.

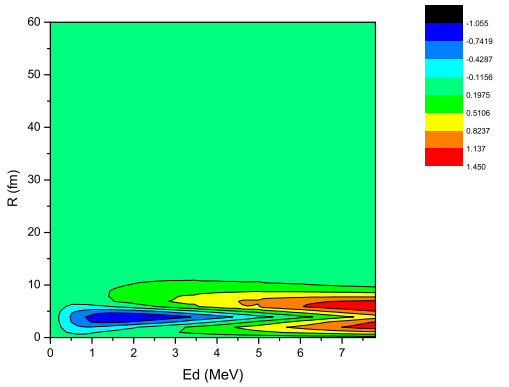


Figure 3. Contour plot of the dipole coupling matrix elements between an $l_f = 2$ scattering state and the g.s., as a function of the relative energy p-$^7$Be and R.

## 3. Couplings to and from the ground state

In the long wave approximation, the monopole matrix elements for the bound state-continuum coupling are zero due to the orthogonality between the bound states and scattering wave functions. As shown in the previous section, the dipole and quadrupole couplings are long-ranged and their range is determined by the Coulomb parts. The nuclear parts are short-ranged. The dipole term decreases as $1/R^2$ and quadrupole as $1/R^3$. In Figs. 2 and 3, we show the contour plot for the dipole couplings of either the $l_f = 0$ or the $l_f = 2$ continuum and the g.s. For $l_f = 0$, the coupling is weak and repulsive at the surface for the lower energies but becomes mildly attractive for the higher energies. The opposite happens for the dipole when $l_f = 2$.

This general picture is valid for the nuclear part (real and imaginary) of the matrix element and the Coulomb part. Naturally the strengths and signs may change, but there is always a structure appearing at low excitation energy and ranges are essentially short, due to the restriction imposed by the bound state wavefunction.

We have also checked the dependence on binding energy of these couplings. We find that the patterns do remain if the binding energy is increased as much as up to 3 MeV. The low energy strength may peak at slightly different values, and the larger the binding, the smaller the strength. All these are characteristics that agree with our previous intuition and therefore the exercise serves also as a check on the use of the bins.

Finally we have also looked at the couplings from the ground state to the continuum for neutron waves instead of proton states. A fictitious system is formed by $n$+$^7$Be, still bound by 0.137 MeV, appropriately adjusting the strength of the Woods Saxon depth in the binding potential. The same depth is then used for the scattering waves, that again do not have Coulomb. The optical potentials are not modified. We find minor changes for the dipole terms, and the quadrupole no longer shows any clear structure.

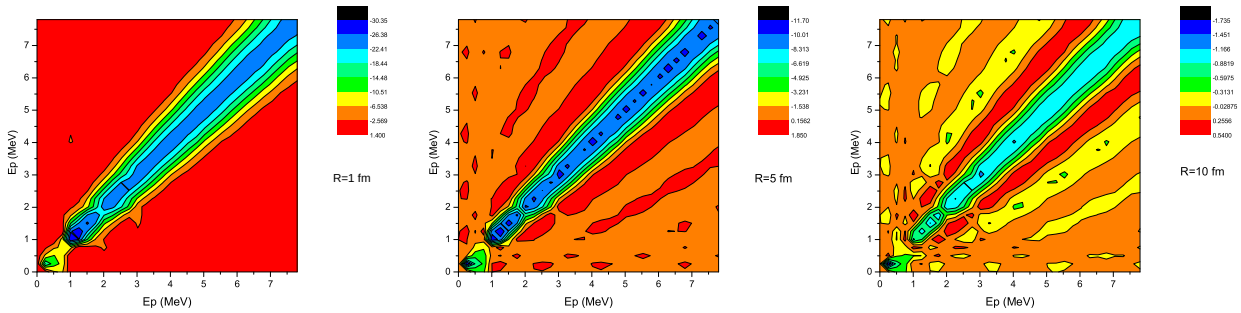


Figure 4. Contour plot of the monopole coupling matrix elements between $l_i = 1$ and $l_f = 1$ scattering states for R=1, 5 and 10 fm, as a function of both relative energies p-$^7$Be.

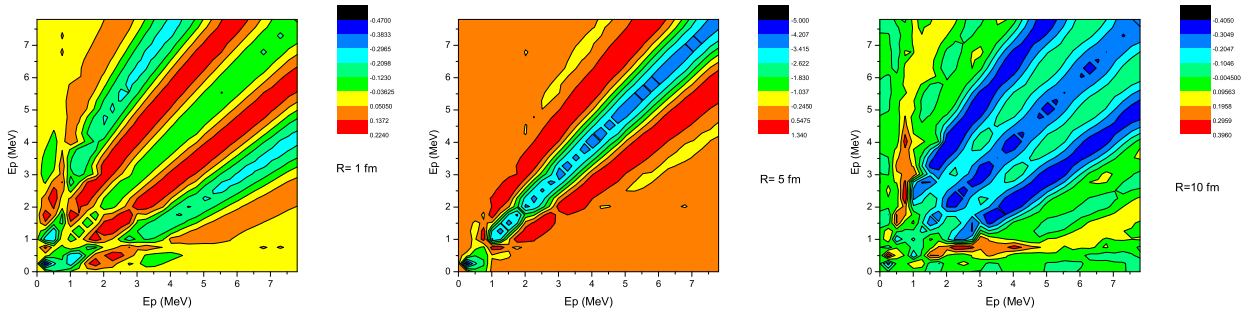


Figure 5. Contour plot of the quadrupole coupling matrix elements between $l_i = 1$ and $l_f = 1$ scattering states for R=1, 5 and 10 fm, as a function of both relative energies p-$^7$Be.

## 4. Continuum-continuum couplings

The calculations show that continuum-continuum couplings are by no means constant over the whole energy window: they tend to be stronger for $E_f \approx E_i$, in perfect agreement with the arguments presented in section 2. Their peaks appear outside the surface region (around 5 fm) and extend out to radii larger than 20 fm.[2] The symmetry pattern of the $E_i$ versus $E_f$ contour plot reflects the multipolarity of the transition considered, as well as the combination of $l_i, l_f$. In order to illustrate these statements, we show the contour plot for transitions between various combinations of $l$-states for 3 different radii: 1, 5, and 10 fm.

We first consider the monopole transition $l_i = 1$ to $l_f = 1$ (Fig.4). Most often, the monopole coupling has no influence in the result: as optical potentials are fit to the elastic data, we generally prefer to have no folding in the diagonal so as not to change the elastic fit. In this work we show the monopole couplings for completeness, and also to help set a trend when increasing multipolarity. One could expect a clear finger print of the p-resonance in these plots. Instead we find there is a ridge along $E_f = E_i$ which is maintained

[2]Here we are considering the radius for which $V_{coupling} \leq E_{binding}$ to define the range of the coupling.

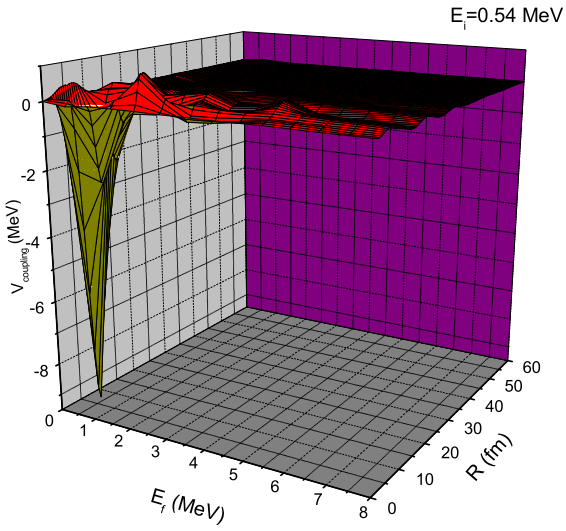


Figure 6. The quadrupole coupling matrix elements between $l_i = 1$ initial scattering state E=0.54 MeV and a final $l_f = 1$ scattering state as a function of the final relative energy p-$^7$Be and R.

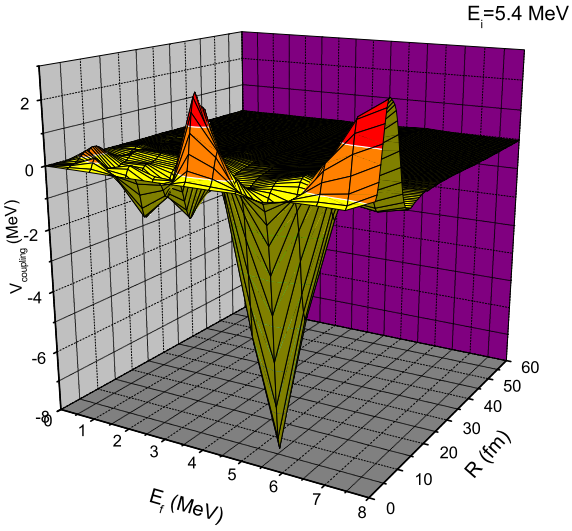


Figure 7. The quadrupole coupling matrix elements between an initial $l_i = 1$ scattering state E=5.4 MeV and a final $l_f = 1$ scattering state as a function of the final relative energy p-$^7$Be and R.

all the way up to the larger energies, which is easy to understand. The monopole term is proportional to the direct overlap of the pair of bins wavefunctions. Consequently, these figures reflect the normalization condition of the wavefunction, which, to a good approximation, are orthogonal for different bin energies [21]. Note that the scales in the three figures are not the same.

In comparison, the quadrupole couplings between p-waves is much weaker but still a few MeV around 5 fm (see Fig.5). Yet, here again, it exhibits a clear ridge for $E_f = E_i$. In the interior the coupling is weak and two parallel lines appear showing that there is also a preference for a slight shift in energy. This ridge structure is also apparent as we move to larger distances.

One can also look closer at the radial dependence by plotting the couplings as a function of $E_f$ and $R$, keeping $E_i$ constant. Such a 3D plot is shown in Fig.(6). Coincidentally there is a strong peak around the p-resonance which could easily be attributed to that. However looking into it with more care, this peak is tied with the initial state energy only $E_i = 0.54$ MeV. We will come back to this point later. At larger energies, due to the rapidly oscillatory behaviour of the wavefunctions, phases can interfere in completely different ways over the energy spectrum and produce a rather bumpy structure such as the one for $E_i = 5.4$ MeV (Fig.7).

The dipole couplings are not symmetric along $E_f = E_i$, since $l_f = l_i$. In fact the set of energies for which the dipole coupling is attractive changes when one moves from the interior to large distances. As can be seen in Fig.(8), the ridge structure is still present

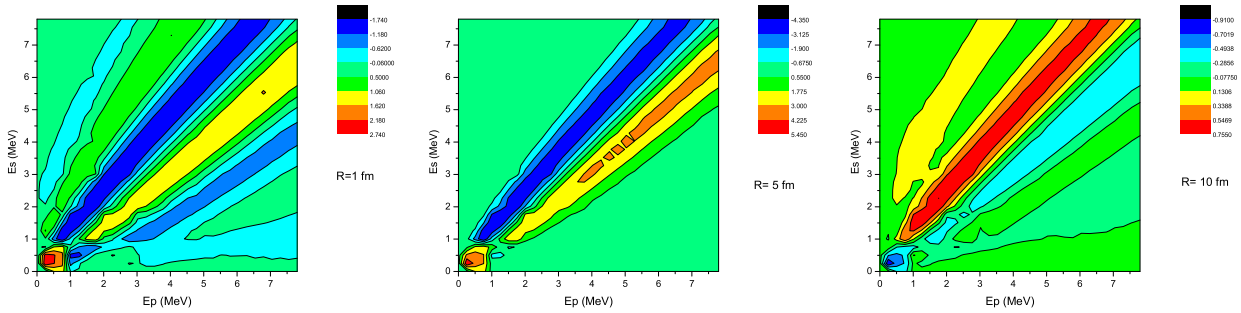


Figure 8. Contour plot of the dipole coupling matrix elements between $l_i = 1$ and $l_f = 0$ scattering states for R=1, 5 and 10 fm, as a function of both relative energies p-$^7$Be.

but no longer runs through $E_f = E_i$; it has been shifted to slightly higher final state energies $E_s + \Delta$ and a nearly symmetrical valley has appeared on the other side $E_s - \Delta$ (for d-waves the opposite is seen).[3]

We also show the 3D plot for the couplings between an initial $E_p = 3$ MeV scattering bin and the s-wave continuum as a function of relative final energy and the distance to the target $R$ (Fig.9). The phases interfere producing both destructive and constructive effects. A similar example for a d-wave final state in shown in Fig.(10). As the initial energy increases, the strength of the couplings also shift to larger $E_f$. So there is always a preference for closer energies although the maximum as we have seen, is not always at $E_f = E_i$.

Notwithstanding the results above, we should comment on the structures of a smaller scale appearing in the illustrations. The discretization of the continuum into bins intends to map the continuum in an efficient way. It is not exact and therefore small ripples in a 3D plot or spotty features in the contour plot are a result of the chosen discretization and should not be taken as real physics. This feature is illustrated in Fig.(11) where results from the standard discretization are compared with those using a broader bin grid, with half of the number of bins.

Since the nuclear and the Coulomb interactions have different ranges and strengths, some of the features depicted are controlled by the nuclear parts whereas others by the Coulomb. However there is one feature that is present regardless, whether we only calculated the nuclear matrix elements or only the Coulomb matrix elements: the concentration of the strength around the $E_f = E_i$ line for the continuum-continuum transitions.

Coulomb multipole transitions are very weak compared with the nuclear multipole transitions, around the surface region. Of course, since Coulomb is repulsive, the Coulomb couplings have opposite signs from the total and the nuclear. These features are expected to change with heavier targets, where Coulomb becomes dominant.

One can also study the features of continuum-continuum couplings when no nuclear interaction is included in the calculation of the scattering wavefunctions ($core+p$ system). We find that the details of the nuclear interaction in the continuum cannot destroy the characteristics that have been identified, even though there is a p-wave resonance in this

[3]Note that we also found asymmetries for quadrupole transitions when $l_f \neq l_i$.

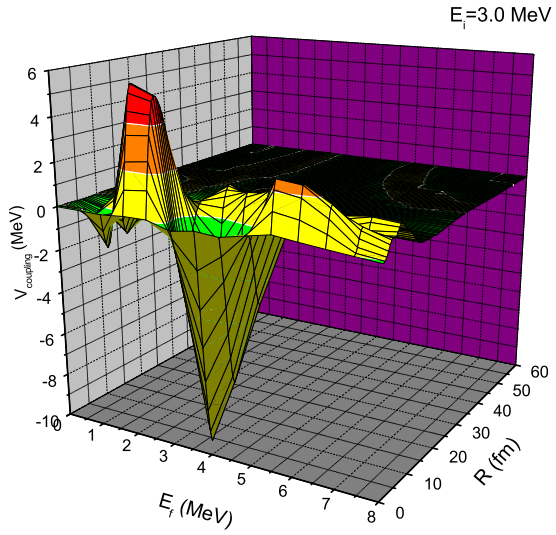


Figure 9. The dipole coupling matrix elements between an initial $l_i = 0$ scattering state E=3.0 MeV and a final $l_f = 1$ scattering state as a function of the final relative energy p-$^7$Be and R.

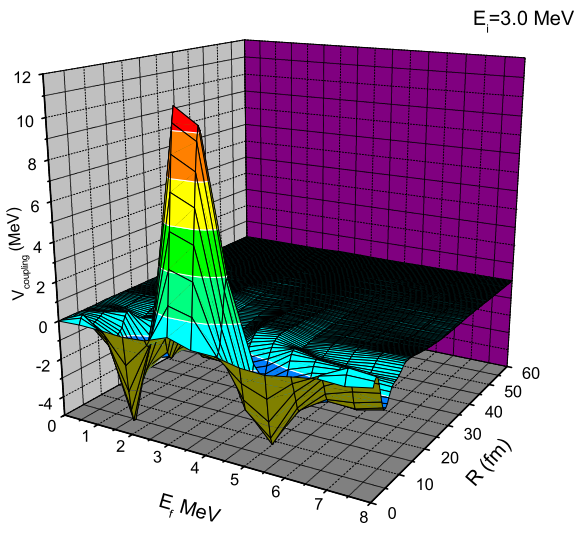


Figure 10. The dipole coupling matrix elements between an initial $l_i = 2$ scattering state E=3.0 MeV and a final $l_f = 1$ scattering state as a function of the final relative energy p-$^7$Be and R.

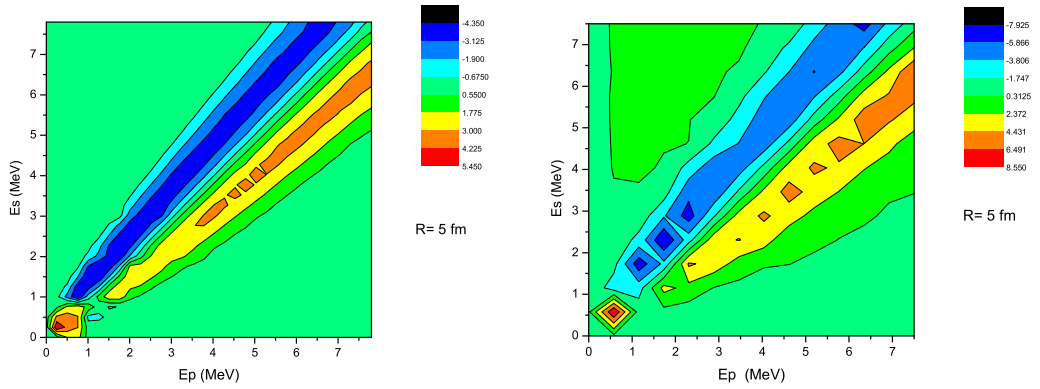


Figure 11. Dipole coupling matrix elements between $l_i = 1$ and $l_f = 0$ scattering states for R= 5 fm: a comparison between couplings using 50 bins on the left, and 25 bins on the right.

$p - core$ system. There is clearly a change in the strengths of the couplings ($\sim 10\%$), but patterns do not change when bins are calculated based on Coulomb waves only.

In addition, the patterns shown above do not change significantly when the binding energy is increased. Given that an increase of the binding energy is achieved by increasing the depth of the nuclear interaction, phase shifts in that situation are no longer the same. However, bin characteristics are matched in a way that the overlap integral keeps the same general features.

If instead of a proton wavefunction we assume the same initial system is a neutron

(as was done in the previous section), the strength of the couplings are slightly modified but the distinctive aspects found before are retained. This is reasonable since the major contribution comes from the $c + T$ interaction which remains exactly the same.

## 5. Conclusions

As a typical case, we have calculated the CDCC couplings for the low energy breakup of $^{8}$B on $^{58}$Ni. We first analise the couplings between the ground state and the continuum and find that regardless of the details of the continuum states, there is always a low energy strength stretching slightly outside the range of the projectile-target interaction.

As to the continuum-continuum couplings, they peak typically around the surface and tend to extend out farther, as there is no bound state to truncate the integral. For the monopole and quadrupole case with $l_i = l_f$, continuum couplings are stronger amongst similar energy pairs. An offset in energy can be found for the cases where $l_i \neq l_f$, as in the dipole coupling. In all these cases, most of the non zero contributions come when the initial and final energies are not far apart.

We also look at variations of binding energy, nuclear versus Coulomb, and neutron versus proton wavefunctions. The general properties described above are not significantly modified.

A standard misconception is that continuum couplings could be reduced to couplings between resonant states. Our work shows that this could not be further from the truth. Our example is good because it contains a strong narrow p-wave resonance at low energy. The various plots shown do not have a clear signature of this resonance. Moreover, if we remove it from the continuum, our conclusions do not change. It is the non resonant continuum that is dictating the rules of the game.

This analysis can help us improve efficiency when it comes to very large CDCC calculations. Given that an initial continuum wave $E_i$ will mainly couple to a final wave that is close in energy ($E_f = E_i \pm \Delta$ where $\Delta$ is small and related to the bin width), and that, as one increases the multipolarity, $\Delta$ increases, it is possible to form blocks in the coupled channel equations, that are no longer coupled, and optimize the performance. Tests along these lines are planned for the near future.

## REFERENCES


1. M. Yahiro and M. Kamimura, Prog. Theor. Phys. **65** (1981) 2046, **65** (1981) 2051.
2. M. Kamimura, M. Yahiro, Y. Iseri, Y. Sakuragi, H. Kameyama and M. Kawai, Prog. Theo. Phys. Suppl. **89** (1986) 1.
3. N. Austern, Y. Iseri, M. Kamimura, M. Kawai, G. Rawitscher and M. Yahiro, Phys. Rep. **154** (1987) 125.
4. A. Mukhamedzhanov and F.M. Nunes, Nucl. Phys. A 708 (2002) 437.
5. F.M. Nunes, Braz. J. Phys. **33** (2003) 195.
6. F.M. Nunes and I.J. Thompson, Phys. Rev. **C57** (1998) R2818.
7. F.M. Nunes and I.J. Thompson, Phys. Rev. C **59** (1999) 2652.
8. J. A. Tostevin, F. M. Nunes, and I. J. Thompson, Phys. Rev. C 63 (2001) 024617.
9. H. Esbensen and G. Bertsch, Phys. Rev. C 59, 3240 (1999)
10. J. J. Kolata et al., Phys. Rev. C 63 (2000) 024616.

11. G.H. Rawitscher, Phys. Rev. **C9** (1974) 2210, **C11** (1975) 1152, Nucl. Phys. **A 241** (1975) 365;
12. J. A. Tostevin et al., Phys. Lett. B 424 (1998) 219.
13. J. Mortimer, I.J. Thompson and J.A. Tostevin, Phys. Rev. **C 65** (2002) 064619.
14. A. M. Moro, R. Crespo, F. M. Nunes, and I. J. Thompson Phys. Rev. C 67 (2003) 047602.
15. N. Austern, M. Kawai, M. Yahiro, Phys. Rev. **C 53** (1996) 314.
16. R.A.D. Piyadasa, M. Kawai, M. Kamimura, M. Yahiro, Phys. Rev. **C 690** (1999) 044611.
17. Y.Iseri, M.Tanifuji, Y.Aoki, and M.Kawai, Phys. Lett. B 265 (1991) 207.
18. Z. Moroz *et al.*, Nucl. Phys. **A381**, 294 (1982).
19. F.D. Becchetti and G.W. Greenlees, Phys. Rev. **182** (1969) 1190.
20. H. Esbensen and G. Bertsch, Nucl. Phys. **A600**, 37 (1996).
21. V.I. Kukulin and O.A. Rubtsova, Theo. Math. Phys. 134 (2003) 404.